

MICRODISTRIBUTION OF OXYGEN IN SILICON AND ITS EFFECTS ON ELECTRONIC PROPERTIES*

H.C. Gatos, B.-Y. Mao, K. Nauka, and J. Lagowski
Massachusetts Institute of Technology
Lexington, Massachusetts

ABSTRACT

The effects of interstitial oxygen on the electrical characteristics of Czochralski-grown silicon crystals were investigated for the first time on a micro-scale. It was found that the generation of thermal donors is not a direct function of the oxygen concentration. It was further found that the minority carrier lifetime decreases with increasing oxygen concentration, on a microscale in "as-grown" crystals. It was thus shown, again for the first time, that oxygen in "as grown" crystals is not electronically inert as generally believed. Preannealing at 1200°C commonly employed in device fabrication, was found to suppress the donor generation at 450°C and to decrease the deep level concentrations.

INTRODUCTION

Oxygen, invariably present in Czochralski-grown crystals, is a most undesirable impurity, as it has not only adverse, but also unpredictably complex effect on Si devices (ref. 1).

Interstitial oxygen in "as grown" crystals has been generally considered to be electronically inert. Upon heat treatment at 450°C, it becomes electronically active and leads to the generation of donors which have been attributed to the formation of Si-O complexes (ref. 2). The concentration of these donors has been related directly to the oxygen concentration (ref. 3). These donors can be annihilated at higher temperatures. Eventually prolonged heat treatment at temperatures exceeding 1000°C leads to microprecipitates of SiO_x (ref. 4).

In our studies we have developed techniques for the direct comparison of oxygen concentration and thermally activated donors on a microscale (ref. 5). Most recently we developed a technique for determining the minority carrier lifetime on a microscale, and thus the means of comparing directly the oxygen concentration to the lifetime. We have found that the thermally activated donors are not necessarily a direct function of the oxygen concentration. More importantly, we found that interstitial oxygen or oxygen in "as grown" crystals is not electronically inert, but it has a pronounced effect on the minority carrier lifetime. Furthermore, heat treatments do not just control the donor concentration, but cause complex electronic interactions with direct implication to Si devices, including photovoltaics.

EXPERIMENTAL

Czochralski-grown B-doped ($\sim 10^{15} \text{ cm}^{-3}$) crystals with an oxygen concentration of about 10^{18} cm^{-3} were employed for the study of the effects of oxygen concentration or oxygen concentration variations on the electronic properties. Longitudinal slices of Si were employed, since pronounced oxygen concentration variations are present

*This work was supported by NASA Lewis Research Center, Grant No. NSG 3017.

along the growth direction (ref. 6). On the other hand, the effects of heat treatment on energy levels within the energy gap were investigated on slices cut perpendicular to the growth direction in which the oxygen concentration variations are relatively small.

Oxygen microprofiles were obtained with scanning IR absorption (ref. 7) and carrier concentration profiles with high resolution spreading resistance measurements.

Lifetime and oxygen concentration microprofiles were obtained with a newly developed double laser arrangement as shown in Fig. 1. The CO₂ laser (9.17 μm wavelength) was employed for obtaining a transmissivity profile from which the oxygen concentration profiles could be determined. A second transmissivity profile--over the identical area--was obtained employing both the CO₂ laser and a YAG laser (10.6 μm wavelength). This transmissivity profile reflected the variation of excess carriers (generated by the YAG laser) superimposed to the variations of oxygen concentration. By subtracting the contribution of the oxygen absorption from the composite transmissivity profile we obtained the variation of the excess carrier concentration. Since the intensity of YAG laser, I, was maintained constant from the variation in excess carrier concentration, Δn, the variation in carrier lifetime, τ, could be directly determined, since

$$\Delta n = (1-R)I\tau$$

where R is the reflectivity coefficient.

Energy levels were determined by Hall-effect measurements as a function of temperature and by deep level transient spectroscopy, DLTS.

RESULTS AND DISCUSSION

In previous communications (ref. 5) we reported that oxygen concentration variations (on microscale) are not directly related to the thermally activated donor concentration variations, and it has been shown that microdefects play an important role in the generation of thermal donors. The analysis of these results is summarized in Fig. 2. The experimental points were obtained from numerous microprofiles of oxygen and thermal donor concentrations (ref. 5b). The line represents the proposed dependence of thermal donor concentration on the fourth power of oxygen concentration (ref. 3). It is seen that measurements on a microscale do not support this dependence and that macroscale measurements do lead to erroneous conclusions.

It has been generally assumed that oxygen in "as grown" Si crystals is electronically inert. For obvious reasons, critical testing of this assumption could not be carried out on the basis of macroscale measurements. However, employing double laser scanning IR absorption revealed, for the first time, that indeed oxygen is electronically active, as seen in Fig. 3. It is seen that the minority carrier lifetime, determined as outlined above, is significantly affected by oxygen. Maxima in the lifetime correspond to minima in oxygen absorption (i.e., in oxygen concentration).

These results are very surprising, as they indicate that interstitial oxygen cannot as yet be understood on a theoretical basis. It must, thus, be assumed, at this time, that oxygen-Si or oxygen-point defect complexes are present along with the interstitial oxygen species.

Attempts were made to study the lifetime variations on a microscale after 450°C heat treatment. However, a pronounced overall decrease in the lifetime made the determination of its variations essentially impossible.

Thus, a series of experiments were initiated to determine the effects of heat treatment at various temperatures (300 to 750°C) on the lifetime employing macroscale measurements. Preliminary results showed that, in general, the lifetime decreases with increasing annealing temperature. However, for a given annealing temperature the lifetime values vary significantly as a function of lifetime measurement temperature (10 to 300 K). Apparently, recombination centers of a different nature are introduced at the various heat treatment temperatures. Work is being pursued to determine the characteristics of the various recombination centers and will be reported in a future communication.

In another series of experiments the effects of preannealing at 1200°C for 30 minutes on subsequent low temperature annealing and on the deep levels in Si were investigated. This type of preannealing is usually employed prior to device fabrication. The results of these experiments are shown in figures 4, 5, and in Table I.

It is seen in Fig. 4 that preannealing decreases the rate of thermal donor generation at 450°C. In fact, conversion from n- to p-type, which takes place without preannealing, does not take place upon preannealing, even after heat treatment for 200 hrs.

In an attempt to clarify the role of high temperature preannealing, the deep level concentrations were determined in "as grown" crystal segments and preannealed. As seen in Fig. 5, two distinct acceptor deep levels were observed in "as grown" Si. The concentration of these levels decreased significantly upon preannealing, as shown in Table I, indicating that these levels do not originate in impurity atoms, but rather in impurity atom-point defect complexes. Although the relationship between the results of Fig. 4 and Table I is not clear at present, it points to the conclusion that the thermal donor generation is a point defect-assisted process.

In summary, oxygen in "as grown" Si or upon heat treatments, employed in device processing, has pronounced effects on electronic properties controlling device performance. These effects appear to be the result of oxygen interactions with point defects or point defect complexes. Identifying the nature and achieving control of these interactions should prove of paramount importance in optimizing device performance and stability.

REFERENCES

1. See, for example, Semiconductor Silicon 1981, edited by Huff, H.R.; Krieger, R.J.; and Takeishi, Y.: The Electrochemical Society, Pennington, N.J.
2. Kaiser, W.: Electrical and Optical Properties of Heat-Treated Silicon. Phys. Rev., vol. 105, no. 6, 1957, pp. 1751-1756.
3. Kaiser, W.; Frisch, H.L.; and Reiss, H.: Mechanism of the Formation of Donor States in Heat-Treated Silicon. Phys. Rev., vol. 112, no. 5, 1958, pp. 1546-1554.
4. Yang, K.H.; Anderson, P.; and Kappert, H.: Identification of Oxide Precipitates in Annealed Silicon Crystals. Appl. Phys. Lett., vol. 33, no. 3, 1978, pp. 225-227. Murgai, A.; Chi, J.-Y.; and Gatos, H.C.: Microdistribution of

Oxygen in Silicon. J. Electrochem. Soc., vol. 127, no. 5, 1980, pp. 1182-1186.

5. (a) Rava, P.; Gatos, H.C.; and Lagowski, J.: Correlation of Oxygen Concentration and Activated Oxygen Donors in Silicon Crystals on a Microscale. J. Appl. Phy. Letters, vol. 38, no. 4, 1981, pp. 274-276. (b) Gatos, H.C.; Rava, P.; and Lagowski, J.: Distribution of Oxygen in Silicon and Its Effects on Electronic Characteristics on a Microscale. Space Photovoltaic Research and Technology, 1980. NASA Conference Publication 2169.
6. Murgai, A.; Gatos, H.C.; and Westdorp, W.A.: Effect of Microscopic Growth Rate on Oxygen Distribution and Swirl Defect Distribution in Czochralski-Grown Silicon. J. Electrochem. Soc., vol. 126, no. 12, 1979, pp. 2240-2245.
7. Jastrzebski, L.; Lagowski, J.; and Gatos, H.C.: Quantitative Determination of the Carrier Distribution in Semiconductors by Scanning IR Absorption: Si. J. Electrochem. Soc., vol. 126, no. 2, 1979, pp. 260-263.

TABLE I. - DEEP ACCEPTOR LEVELS IN Si AND THE EFFECT OF PREANNEALING AT 1200°C FOR 30 MINUTES

	Sample	0.19 eV	0.43 eV
As Grown	A	2.4×10^{11}	1.2×10^{11}
	A'	2.7×10^{11}	1.2×10^{11}
Preannealing	B	7.2×10^{10}	7.2×10^{10}
	B'	undetectable	undetectable

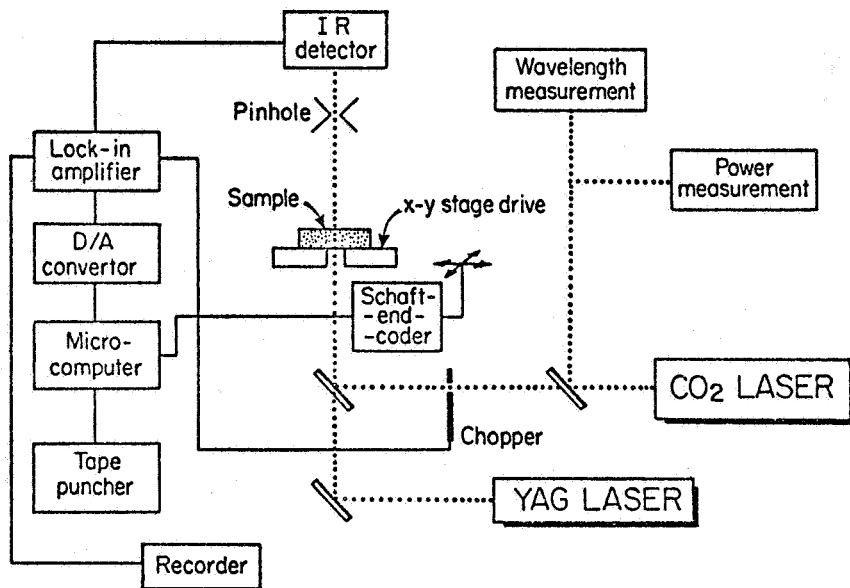


Figure 1. Schematic representation of double laser scanning absorption.

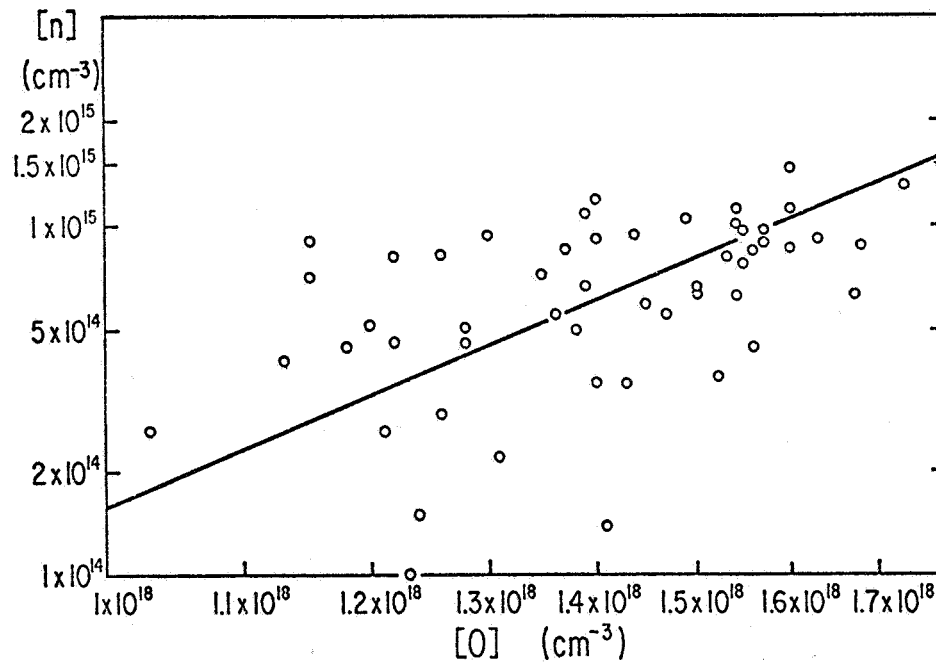


Figure 2. Thermal donor concentrations activated by heat treatment at 450°C for 4 hrs as a function of oxygen concentration. Straight line represents proposed relationship between thermal donor and oxygen concentrations (ref. 3).

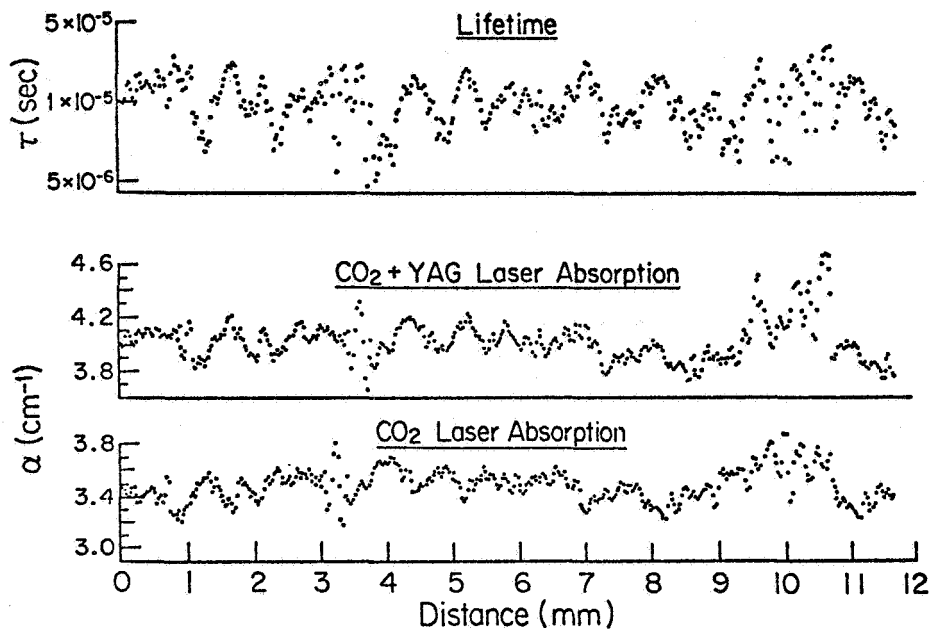


Figure 3. Variation of oxygen concentration (CO_2 laser absorption) and lifetime as a function of distance along the growth direction (see text).

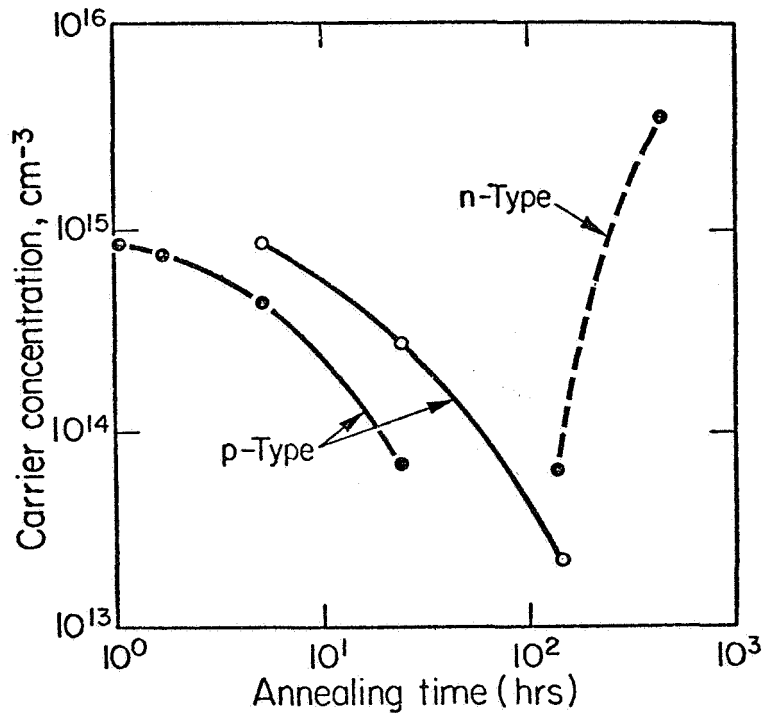


Figure 4. Carrier concentration as a function of annealing time at 450°C
 ● "as grown" Si; ○ preannealed at 1200°C for 30 minutes.

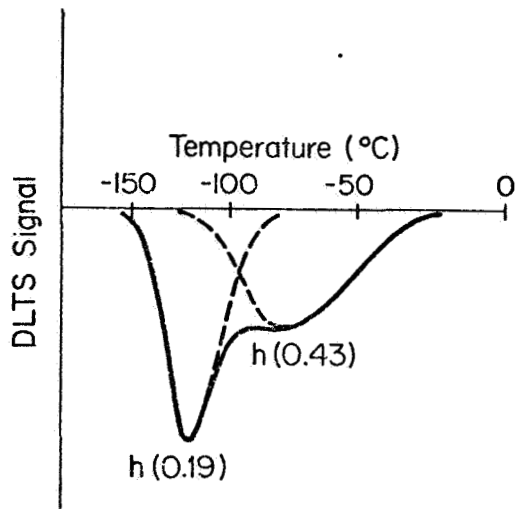


Figure 5. DLTS spectrum of "as grown" Si.

EFFECTS OF INJECTION CHARGE DISTRIBUTION ON THE PERFORMANCE OF RADIATION DAMAGED, HIGH RESISTIVITY CELLS

I. Weinberg, C. Goradia*, and C.K. Swartz
NASA Lewis Research Center
Cleveland, Ohio

Extended Abstract

Previous results indicate that, contrary to expectations, for sufficiently high cell base resistivities, the radiation resistance of silicon solar cells decreases as cell resistivity increases (ref. 1). This result was observed for n^+pp^+ cells of 84 and 1250 Ω -cm base resistivities, the data being analyzed using a theory valid only under open circuit conditions (ref. 2). From this a qualitative argument was presented to show that the increased degradation was due primarily to an increased voltage drop in the cells' base region (ref. 1). In the present case we use an analytical model, valid over all cell voltages, to place our previous qualitative conclusions on a firmer quantitative basis. Since loss of conductivity modulation is attributable to the behavior of the base injected charge distribution (ref. 3), we pay particular attention to this factor in our present treatment of the data.

Normalized maximum power as a function of fluence, after irradiation by 1 MeV electrons, is shown in figures 1 and 2. Also shown in figure 1 are the data for a 10 Ω -cm silicon cell with BSF (ref. 4). From both figures it is readily seen that in the resistivity range shown, as cell base resistivity increases the radiation induced degradation increases. This is the reverse of the behavior usually observed for cells in the lower resistivity ranges (ref. 4).

Base majority carrier concentrations, in the present unirradiated cells, are lower than the injected minority carrier concentrations at air mass zero. Hence, the usual low injection models do not apply. For this reason, we have developed a model, valid for both high and low injection levels, to use in treating the present data. Additional details have been presented in a previous publication (ref. 5). The model takes into account nonuniform optical carrier generation, band gap narrowing, generation, and recombination in the n^+p space charge region, wavelength-dependent reflection coefficients, and ohmic and Dember voltage contributions in the base region.

Schwartz et al. (ref. 3) have shown the importance of the base minority carrier distribution as a factor in cell degradation under high injection conditions. Calculations for a BSF cell under these conditions show that, with increasing cell current, the injected carrier concentration at the back junction decreases, with the region of low concentration progressively extending toward the front junction (ref. 3). In the present case, a similar situation holds for the high resistivity cell as diffusion length decreases with fluence (fig. 3). At the lower fluences the cell of figure 3 is in high injection. With increased fluence, the injected carrier concentration decreases, and portions of the cell near the back junction are in low

*Dept. of Electrical Engineering, Cleveland State University, Cleveland, Ohio.

injection. As the injected carrier concentration is lowered, the ohmic voltage drop across the cells' base region is anticipated to contribute significantly toward cell degradation. However, as cell thickness decreases, the diffusion lengths are still large enough, compared with cell thickness, that one does not encounter the gradient of injected carrier concentration seen in figure 3. This is illustrated in figure 4 for the thinnest higher resistivity cell. In this case, although the injected carrier concentration is higher than the base concentration, the cell base resistivity is still high enough to contribute a significant ohmic drop in the cells' base region. Behavior of the injected carrier concentration for the thicker 84 Ω -cm cell is shown in figure 5. In this case the cell is near the high injection condition at low fluence, the entire cell being in low injection at the higher fluences. Similar calculations of charge densities were carried out for all cells except the 10 Ω -cm cell of figure 1. These served as the basis for calculating components of the cell output voltage V where

$$V = V_1 + V_2 - V_{DEM} - V_{ohmic} - IR_s \quad (1)$$

where V_1 and V_2 are the front and rear junction voltages, V_{DEM} is the Demer potential, V_{ohmic} is the ohmic voltage drop across the cells' base region and IR_s is the remaining series resistance voltage drop due to cell components other than the base. The computed voltage drops are shown in figures 6 and 7 for the thicker cells of both resistivities. The ohmic drop is seen to be the dominant factor in degradation of the higher resistivity cell. As expected, the ohmic contribution diminishes with decreased cell resistivity but remains a significant factor in the thicker low resistivity cell. As shown in figure 8, this component diminishes with cell thickness, but is still significant in the thinner high resistivity cell, and is nontrivial in the thinner lower resistivity cell.

The present results indicate that as cell resistivity increases, the base injected minority carrier distributions, leading to lack of conductivity modulation, are increasingly significant factors in radiation-induced cell degradation. Although, for the cells presented here, degradation increases with increased resistivity, cells of lower resistivity show decreased degradation with increased resistivity (ref. 4). Thus, there appears to be a trade-off between decreased radiation-induced degradation due to decreased dopant concentration and the degrading effects of ohmic voltage drops.

REFERENCES

1. Weinberg, I.; Goradia, C.; Swartz C. K.; and Herman, A. M.: Performance of High Resistivity n^+pp^+ Silicon Solar Cells Under 1 MeV Electron Irradiation. Proc. 15th IEEE Photovoltaic Specialists Conference, 1981, pp. 484-489.
2. Wu, C.-Y. and Shen, W-Z: The Open Circuit Voltage of Back-Surface-Field (BSF) p-n Junction Cells in Concentrated Sunlight. Solid State Electron., vol. 23, 1981, pp. 219-216.
3. Schwartz, R. J.; Lundstrom, M. S.; and Nasby, R. D.: The Degradation of High-Intensity BSF Solar-Cell Fill Factors Due to a Loss of Base Conductivity Modulation. IEEE Trans. on Electron Devices, vol. ED-28, 1981, pp. 264-269.
4. Tada, H. Y.; and Carter, J. R., Jr.: Solar Cell Radiation Handbook. NASA JPL Publication 77-56, Chapt. 3, 1977.
5. Goradia, C.; Weinberg, I.; and Baraona, C.: A Theory of the N-I-P Silicon Solar Cell. Proc. 15th IEEE Photovoltaic Specialists Conference, 1981, pp. 855-860,

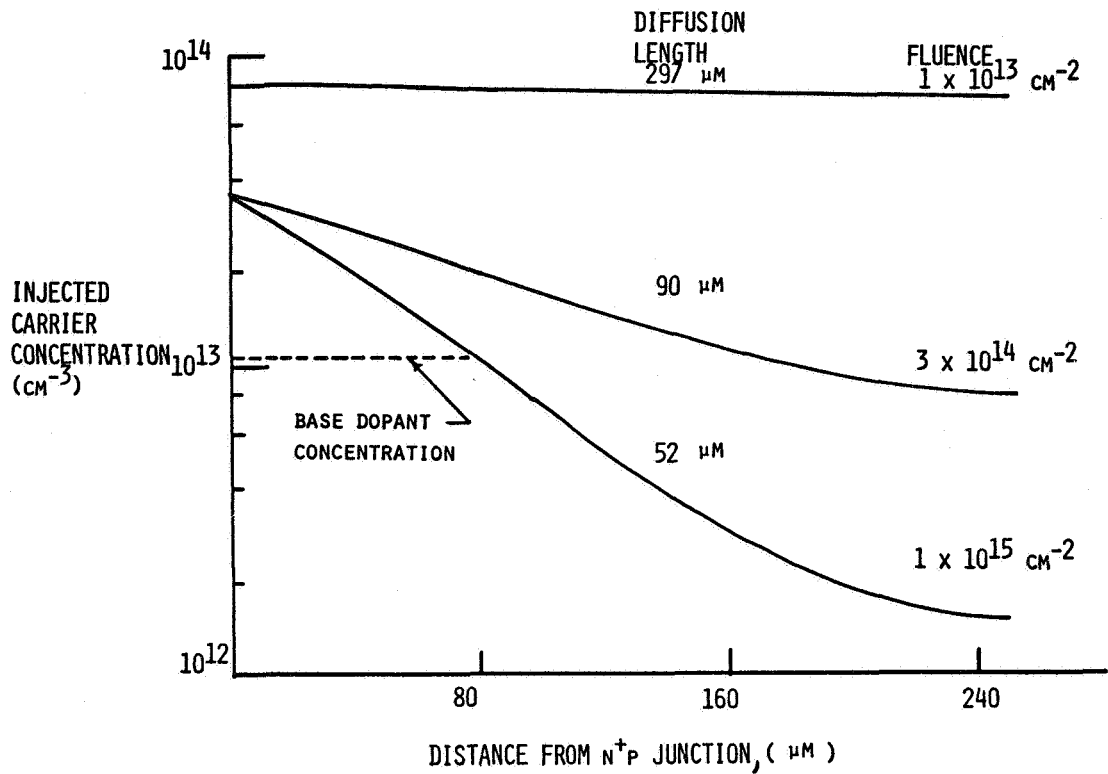


Figure 3. - Injected carrier concentration in cell's base region at P_{max} .
 $\rho = 1250 \Omega\text{-cm}$; thickness = $250 \mu\text{m}$.

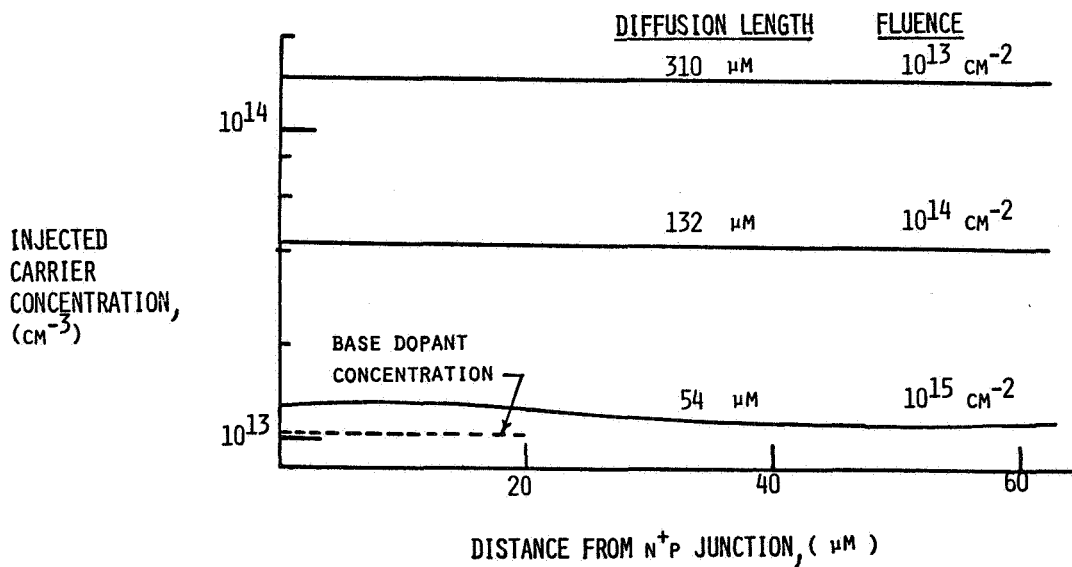


Figure 4. - Injected carrier concentration in cell's base region at P_{max} .
 $\rho = 1250 \Omega\text{-cm}$, thickness = $61 \mu\text{m}$.

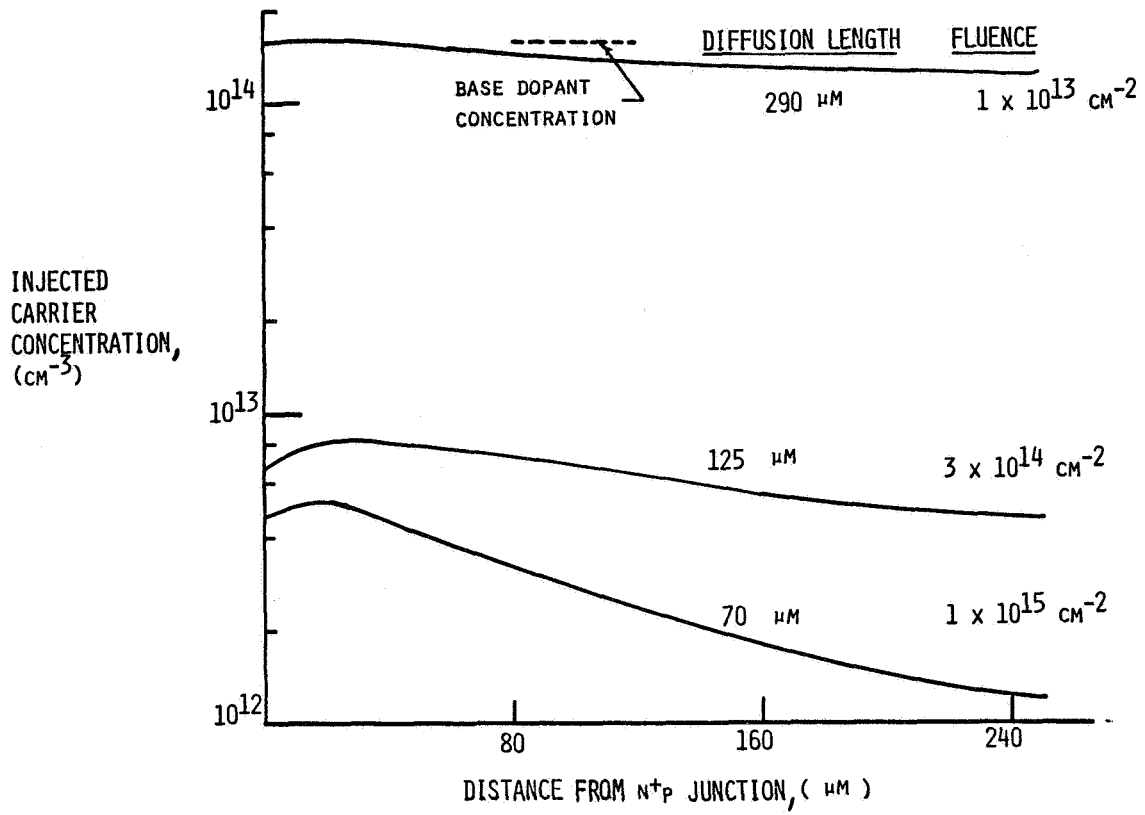


Figure 5. - Injected carrier concentration in cell base. $\rho = 84 \Omega\text{-cm}$; $t = 250 \mu\text{m}$.

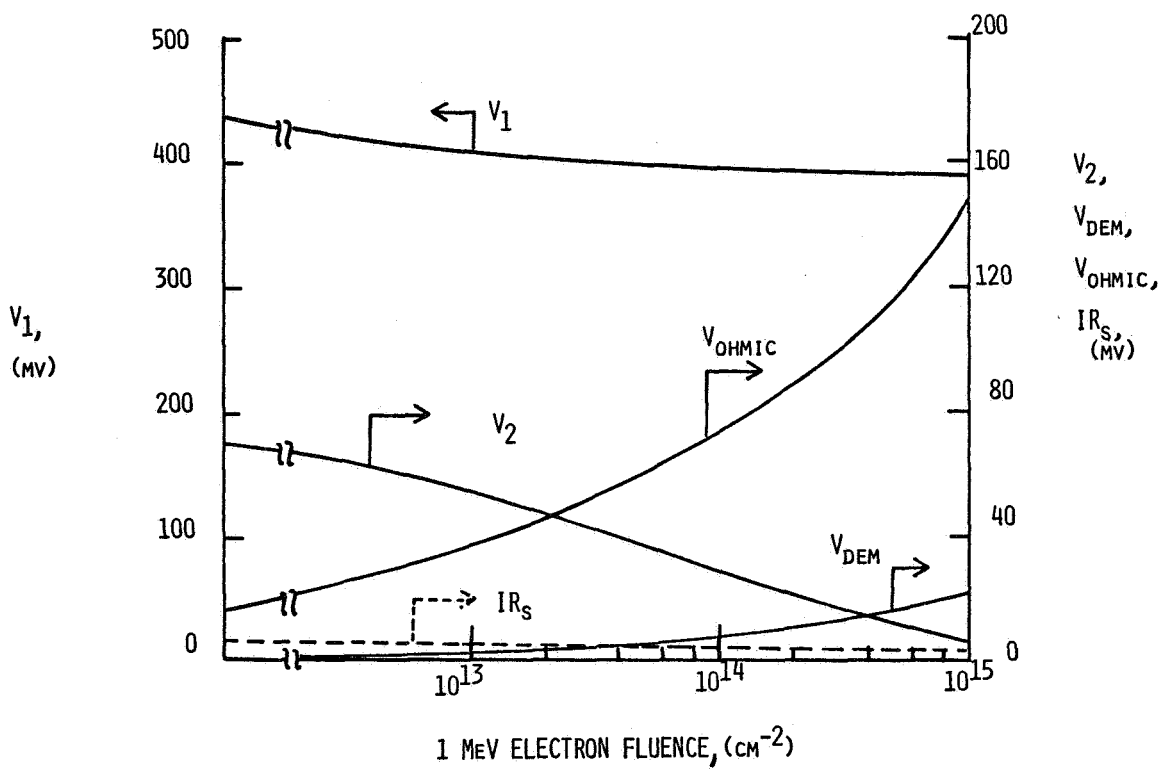


Figure 6. - Voltage components at P_{max}. $\rho = 1250 \Omega\text{-cm}$, $t = 250 \mu\text{m}$.

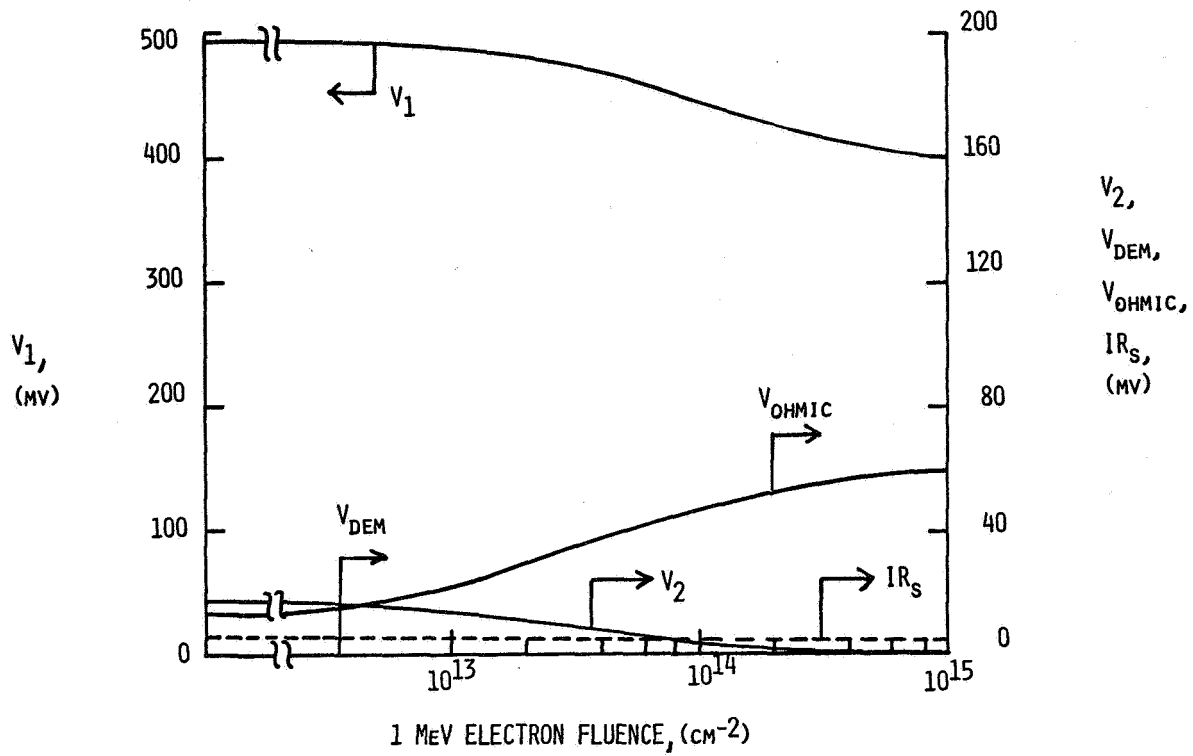


Figure 7. - Voltage components at P_{max} . $\rho = 84 \Omega\text{-cm}$; $t = 250 \mu\text{m}$.

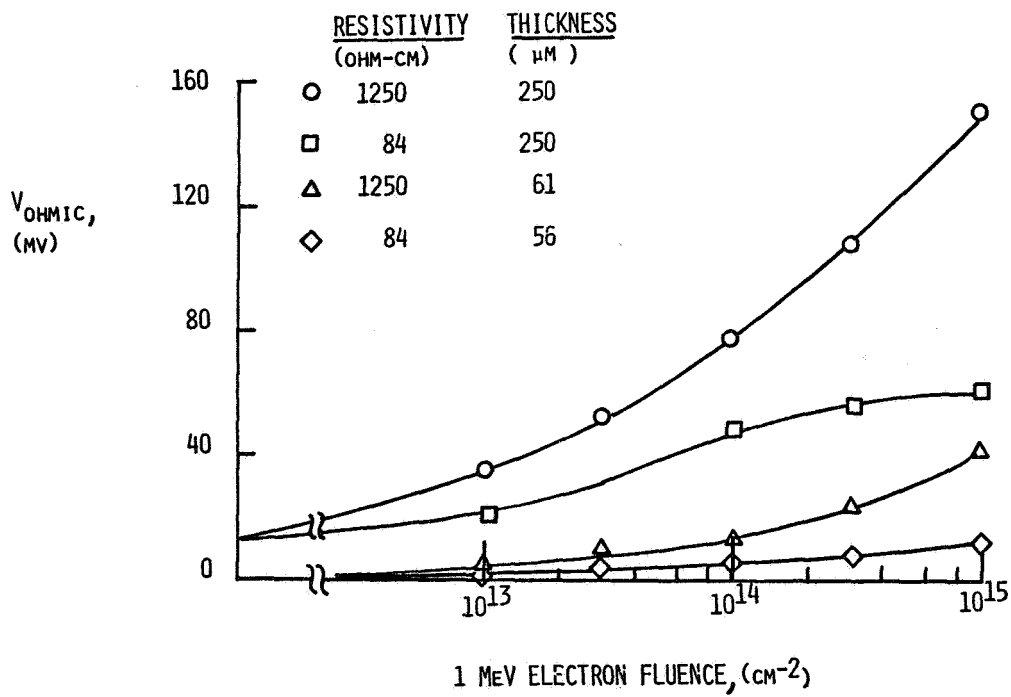


Figure 8. - Ohmic voltage component - all cells.

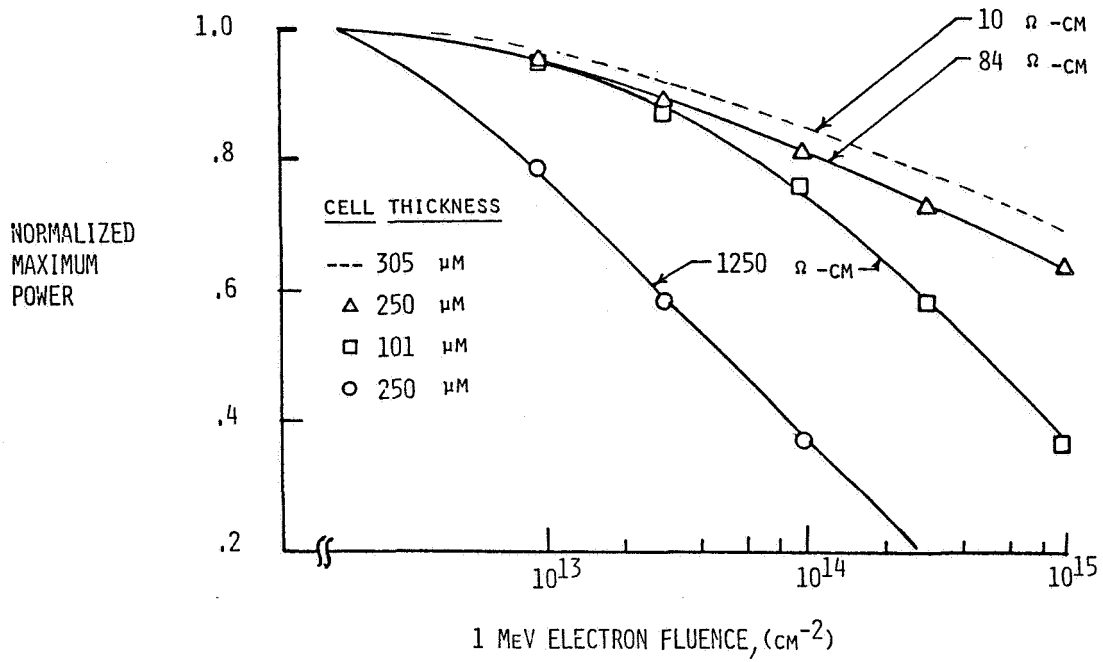


Figure 1. - Normalized maximum power versus 1-MeV electron fluence for high resistivity n^+pp^{++} cells. Cell thickness, 101 to 305 μm.

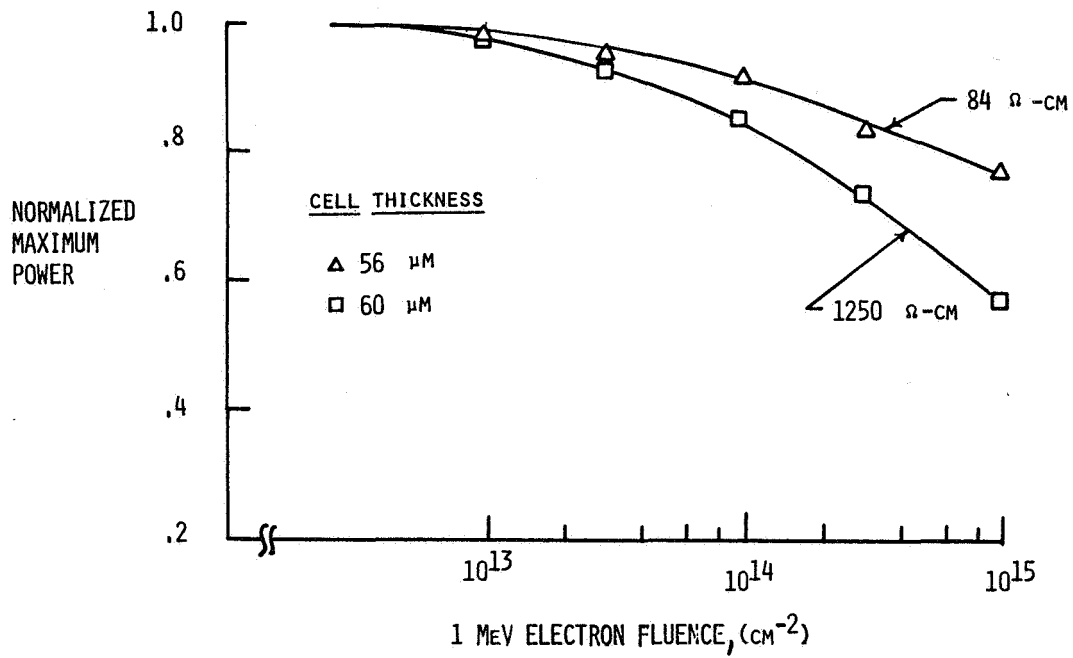


Figure 2. - Normalized maximum power versus 1-MeV electron fluence for high resistivity n^+pp^+ cells.